Journal of Sound and Vibration (2001) **247**(4), 655–672
doi:10.1006/jsvi.2001.3768, available online at http://www.idealibrary.com on IDEAL®

PITCHFORK-TYPE BIFURCATIONS IN A PARAMETRICALLY EXCITED, PD-CONTROLLED PENDULUM OR MANIPULATOR

T. P. Bucklaew and C.-S. Liu

Department of Mechanical and Aerospace Engineering, State University of New York at Buffalo, Buffalo, NY 14260, *U.S.A.*
E-mails: *bucklaew@eng.buffalo.edu*; *chingliu@eng.buffalo.edu*

(*Received* 9 *October* 2000, *and in final form* 13 *April* 2001)

In this paper, the effect of a vibrating support base upon the behavior of a simple robotic manipulator with PD control is examined. The physical system to be controlled, i.e., the plant, is modelled initially as an inverted pendulum. The vibrating support generates a time-periodic parametric excitation of the controller–plant system that is shown, under certain operating conditions, to produce a bifurcation in the steady state motion, whereby a globally stable limit cycle encircling the target position is replaced by two offset, and competing, periodic attractors. The basins of attraction of each are sketched, and predictive criteria for the bifurcation to occur are presented in terms of key system parameters. As the resulting steady state error can be quite large, the post-bifurcation regime of motion often implies a total control failure and is therefore of significant interest. The extrapolation of the results obtained for a higher ordered model is discussed, and the bifurcation boundary is mapped in the disturbance parameter plane for a two-degrees-of-freedom manipulator model.

1. INTRODUCTION

The non-autonomous pendulum is a common paradigm of non-linear dynamics, despite its low dimensionality and outward simplicity. Chaotic oscillations, and other phenomena, are well documented for cases of both time-periodic driving input [1, 2] as well as parametric excitation [3, 4]. The dynamic behavior of the *controlled* pendulum in the presence of a time-dependent disturbance, however, has received significantly less attention.

In one degree of freedom, the pendulum adequately models the plant of a simple robotic system. This analogy can be readily extended as additional degrees of freedom are introduced, as higher ordered, *revolute*, serial manipulators are generally synonymous with a structure of linked pendulum, as discussed below. Regulating the set-point motion of such a plant, regardless of dimension, is a problem whose classic solution is the proportional plus differential (PD) controller, with some form of gravity compensation.

PD-type controllers remain in widespread use due, in part, to their simplicity and general robustness. The sensitivity of a controller–plant system to a time-periodic disturbance is an important consideration, especially in industrial applications, where error tolerances are low and vibration isolation may be difficult. Typical performance requirements are such that the appearance of any appreciable steady state oscillation or offset error can represent a control failure.

0022-460X/01/440655 + 18 $35.00/0

A traditional approach in control applications is to model a potential disturbance as an additional input to the forward control loop, resulting in a driving vibration that is non-parametric in nature. One convenient advantage of such a formulation is that it may permit the sensitivity of the controller to input disturbance to be expressed through a disturbance transfer function. Investigation of alternative forcing models, however, has revealed that more complex behavior than otherwise anticipated may be a potential concern for PD-controlled manipulators.

Recent research by Ravishankar and Ghosal [5], Lankalapalli and Ghosal [6], and Mahout *et al.* [7], has explored the potential for chaotic oscillations in certain PD-controlled robotic manipulators of two and three degrees of freedom. In the referenced work, the controller tracks a desired time-periodic trajectory, and therefore is itself the source of non-autonomous terms. The selective dimensionality of such studies might seem to imply that the non-linear coupling between manipulator links is a key factor enabling mathematically intriguing dynamics to occur. It will be shown below that this is not necessarily the case, however, and that controller effectiveness can also be jeopardized, even in the lowest order model and for set-point regulation, when vibrations are transmitted through the base support.

The specific contribution of this article is to demonstrate that a time-periodic base oscillation of a robotic manipulator, or a generic inverted pendulum with control, can, in some circumstances, produce large offset errors and effective control failure as a result of a sudden, parameter-dependent change in the orbit structure of the system, i.e., a bifurcation. Although minor steady state oscillations are present as a result of the root disturbance, this bifurcation is most accurately described as pitchfork type [8]. More explicitly, a globally state limit cycle centered about the desired equilibrium is destroyed and succeeded by two offset limit cycles for parameter values exceeding a critical threshold. The amplitude and frequency of the excitation, as well as the ratio of the maximum weight-induced torque to the proportional error signal gain, are shown to directly influence the location of the bifurcation.

The organization of this article is as follows. In the next section, the mathematical model for plant, controller, and disturbance are developed, resulting in a statement of the governing equation for the non-autonomous controller–plant system. In section 3, the dynamic behavior is analyzed, and bifurcation diagrams are presented. Basins of attraction for competing attractors are sketched in section 4. The response of a two-degrees-of-freedom model is considered in section 5, and the bifurcation boundary is mapped in the disturbance parameter plane. Conclusions directly follow.

2. GOVERNING EQUATION

2.1. CONTROLLER–PLANT SYSTEM

An n-degree-of-freedom, rigid, frictionless robotic manipulator, or serially linked system of pendula, can be described by Lagrange's equation

$$\frac{\mathrm{d}}{\mathrm{d}t}\frac{\partial L}{\partial \dot{\theta}_i} - \frac{\partial L}{\partial \theta_i} = u_i, \tag{1}$$

where u_i is an as-of-yet unspecified control law and $i = 1, \ldots, n$. The Lagrangian is defined as $L = T - V$, where the total kinetic and potential energies are the sums of that for the component links, i.e., $T = \sum_{i=1}^{n} T_i$ and $V = \sum_{i=1}^{n} V_i$ respectively. The resulting equation of motion in the joint-space is typically expressed as [9]

$$\mathbf{H}(\boldsymbol{\theta})\ddot{\boldsymbol{\theta}} + \mathbf{C}(\dot{\boldsymbol{\theta}}, \boldsymbol{\theta})\dot{\boldsymbol{\theta}} + \mathbf{g}(\boldsymbol{\theta}) = \mathbf{u} + \mathbf{D}(\boldsymbol{\theta}, \mathbf{t}), \tag{2}$$

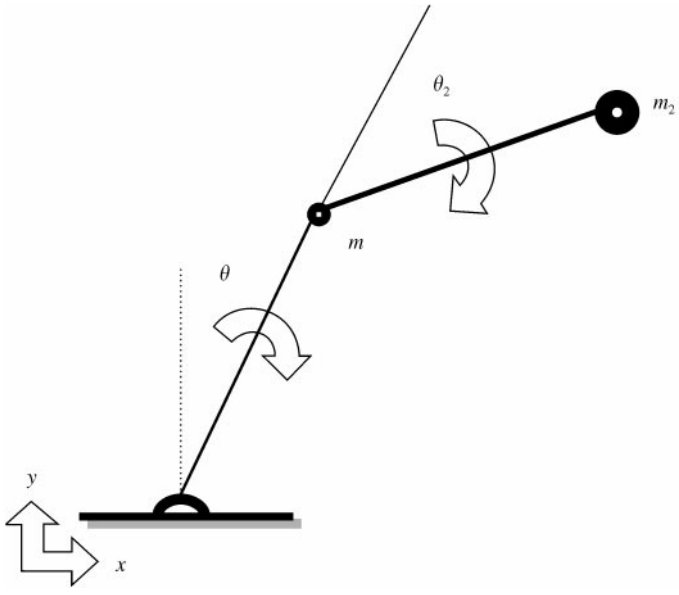

Figure 1. RR-robot operating in a vertical plane. The joint-space is defined by (θ, θ_2), while base vibrations are considered along a horizontal Cartesian axis.

where $\boldsymbol{\theta} \in \Re^n$ is a vector of joint variables and $\mathbf{D}$ is a disturbance vector. The $n \times n$ matrices of equation (2) can be identified, from left to right, with inertial and centripetal forces, respectively, while $\mathbf{g}$ is the n vector of gravitational torque.

In this paper, the discussion is largely limited to purely revolute systems of form (2) when the disturbance vector arises as a result of a horizontal oscillation $X(t)$ of the base support. The vector of joint angles $\boldsymbol{\theta}$ identifies the manipulator position in a vertical plane defined by a horizontal x-axis and vertical y-axis, as illustrated in Figure 1 for the case of a two-bar linkage. A numeric subscript is employed to denote properties of the secondary link, while that of the primary link remain unadorned.

The problem of set-point position regulation of plant (2) is now considered. The disturbance $\mathbf{D}(\boldsymbol{\theta}, t)$ is regarded as unanticipated and for the moment is ignored. The uncontrolled plant model, if autonomous, possesses fixed equilibria of mixed stability, with an unstable saddle node at the origin for purely revolute systems. The objective of the controller in this situation is to produce a single, globally asymptotically stable equilibrium, whose location is dependent upon a command input. The traditional PD controller accomplishes this by utilizing a linear feedback of errors in both position and velocity to drive the system to the desired target state. As the manipulator operates in a vertical plane, gravitational effects are a concern that cannot be neglected. A rather basic solution is to explicitly cancel these forces with an additional control term in the feedback loop that estimates the torque induced by gravity based upon the plant model and the current measurement of the joint angle. This entails, however, an increasingly cumbersome closed-loop calculation as system order increases that can, in practical terms, adversely affect the sampling speed and therefore degrade controller effectiveness.

A more efficient method is afforded by use of a constant compensation term equivalent to the gravitational torque at the target state, which is known *a priori*. PD control with desired gravity compensation [10, 11] has been shown to provide an asymptotically stable equilibrium at the target state provided the proportional gains are chosen sufficiently large

to provide an actuating effort able to counterbalance the linkage weight. The controller structure is illustrated by means of a block diagram in Arimoto [12]. The control law can be given as

$$\mathbf{u} = -\mathbf{K}_d\dot{\boldsymbol{\theta}} - \mathbf{K}_p\tilde{\boldsymbol{\theta}} + \mathbf{g}(\boldsymbol{\theta}_d), \tag{3}$$

where $\boldsymbol{\theta}_d$ is the input target position, $\tilde{\boldsymbol{\theta}} = \boldsymbol{\theta} - \boldsymbol{\theta}_d$ is the error signal, and $\mathbf{K}_p$ and $\mathbf{K}_d$ are diagonal, positive-definite matrices of error signal gains.

In the absence of disturbance, it can be seen [11] that the controlled system possesses a globally, asymptotically stable equilibrium at $\boldsymbol{\theta} = \boldsymbol{\theta}_d$, provided that the payload estimate is accurate and the gains of $\mathbf{K}_p$ are sufficient to provide a control effort greater than the gravitationally induced torque. If these conditions are not met, then control effectiveness can be jeopardized. For instance, if the estimate of the payload inertia is not accurate, gravitational effects will be incompletely compensated. As a result, there will be an offset error in the steady state position, proportional to the estimation error, such that $\boldsymbol{\theta}_d$ is no longer the equilibrium point. It has been shown, however, that the resulting offset equilibrium remains globally asymptotically stable [13]. Under-actuation poses an additional set of difficulties, as discussed by Kelly [11].

The focus of this study, in contrast, is the effect of time-dependent forcing upon a controller–plant system that would otherwise be well behaved in the absence of such disturbances. In the analysis to follow, it shall be assumed that the inertia is known exactly, and also that $\mathbf{K}_p$ is chosen sufficient to produce an asymptotically stable equilibrium at $\boldsymbol{\theta}_d$ when $X(t)$ vanishes. Of primary interest, consequently, is how controller performance is affected qualitatively by the introduction of the parametric excitation $\mathbf{D}(\boldsymbol{\theta}, t)$, as well as by changes in key system parameters. Specifically considered below are cases of $n = 1$ and 2, where a transformation to a dimensionless time scale is employed to reduce the number of parameters.

2.2. DIMENSIONLESS MODEL IN ONE d.o.f.

Although the bulk of practical robotic manipulators possess multiple links, a simpler model is initially examined. The single-degrees-of-freedom case is quite illuminating with respect to the dynamics of this particular class of problem, and allows for a more direct treatment than that afforded by a higher ordered system at the outset. Additionally, it clarifies unambiguously that the dynamic behavior discussed is inherent to the parametrically excited system, and is not the product of a coupling or Coriolis non-linearity introduced at higher order that may be more or less significant dependent upon the control speed desired. Extrapolation of the results obtained by a two-degrees-of-freedom model will be addressed subsequently, and it will be shown that similar qualitative behavior is exhibited.

Consider an *inverted*, rigid, frictionless pendulum of length l, payload mass m, and inertia J as the plant. The pendulum is free to rotate in the co-ordinate θ in a vertical plane defined by a horizontal x-axis and a vertical y-axis, as previously discussed. The payload, or end-effector, position (x, y) is constrained such that $x = l\sin\theta + X(t)$ and $y = l(1 + \cos\theta)$, where $X(t)$ represents the horizontal motion of the base support. The Lagrangian is therefore expressed as $L = \frac{1}{2}m(\dot{x}^2 + \dot{y}^2) - mgy$, and the forced controller–plant system (2)–(3) reduces [14] to

$$J\ddot{\theta} + K_d\dot{\theta} + K_p\tilde{\theta} + mgl(\sin\theta - \sin\theta_d) = -ml\,\ddot{X}(t)\cos\theta, \tag{4}$$

where an overdot represents differentiation with respect to time.

Two assumptions are made for the sake of simplicity in the subsequent analysis. First, the desired target state is chosen as $\theta_d = 0$, the unstable saddle node in the uncontrolled, undisturbed plant. Second, the disturbance oscillation is presumed to be of a simple periodic form, i.e., $X(t) = X_0 \cos \omega t$. Numerical simulations conducted with non-zero θ_d demonstrate that there is no apparent loss of generality introduced by the former analytical convenience.

Equation (4) can be simplified by introducing a co-ordinate change to dimensionless variables. The most convenient means of doing so is by scaling t by the natural frequency of the pendulum such that

$$\tau = \sqrt{\frac{K_p}{J}}\, t. \tag{5}$$

Subsequently, $\ddot{X}(\tau)$ can be expressed in terms of a dimensionless frequency Ω, where $\Omega\tau = \omega t$ or

$$\Omega = \omega \sqrt{\frac{J}{K_p}}. \tag{6}$$

On the basis of the explicit form of the time-dependent terms, and noting that the measure of θ is in radians, the dimensionless governing equation for the single-degree-of-freedom case can be given as

$$\ddot{\theta} + 2\beta\dot{\theta} + \theta = f(\tau)\cos\theta + \gamma \sin\theta \tag{7}$$

with

$$\beta = \frac{K_d}{2\sqrt{JK_p}}, \qquad \gamma = \frac{mgl}{K_p} \tag{8, 9}$$

and

$$f(\tau) = \alpha\Omega^2 \cos(\Omega\tau), \tag{10}$$

where $\alpha = X_0/l$ scales the amplitude of the base motion by the length of the manipulator. As the dimensionless frequency Ω is linearly proportional to the original ω, it can be seen that high-frequency base oscillations, even at low amplitude, can produce a strong parametric forcing. For a rather limited range of physical parameters, i.e., $J > K_p > mgl$. Ω will actually amplify ω in this co-ordinate frame.

For manipulator models, the Cartesian co-ordinates (x, y) of the payload are typically a desired output, though the equation of motion is most conveniently represented in terms of the state variables given in equation (12). In one degree of freedom, the relationship between the two co-ordinate systems is rather straight forward, and little additional discussion is warranted. In higher ordered models, however, it is often necessary for a complete description of the controller–plant system to include an output equation relating the state variables to the desired output.

Given the previously stipulated stability conditions on the proportional gain K_p, it can be seen that $0 < \gamma < 1$. For small γ, the damping ratio, traditionally denoted as ζ, of the controller–plant system is approximated by β. For larger γ,

$$\zeta = \beta/\sqrt{1-\gamma} \tag{11}$$

gives a more accurate approximation. It can be observed, therefore, that as γ increases at fixed β, the control response may become more sluggish. In many common systems, mathematically interesting behavior can be found to occur only for cases of very light damping. In control applications, this is an unlikely condition, given the reasonable performance requirements. As a result, an estimation of the damping ratio is mentioned in order to demonstrate that the dynamic behavior discussed below is applicable to more realistic problems.

2.3. TWO d.o.f. DIMENSIONLESS MANIPULATOR MODEL

In the case of two degrees of freedom, shown in Figure 1, it is again convenient to transform the governing equation to a dimensionless time scale. As the explicit population of the matrices in equation (2) can be found in numerous texts, e.g. reference [15], only the transformed elements are explicitly presented here. The Cartesian position (x, y) of the primary link is as previously given. The manipulator payload is now located at the tip of the secondary link, however, resulting in an output equation

$$\begin{bmatrix} x_2 \\ y_2 \end{bmatrix} = \begin{bmatrix} x + l_2 \sin(\theta_1 + \theta_2) \\ y + l_2 \cos(\theta_1 + \theta_2) \end{bmatrix}. \tag{12}$$

The transformation to a dimensionless time scale τ is employed as defined in equation (5). The parameters α, β, γ, and Ω remain as before, while additional dimensionless ratios of length, mass, and gain are introduced in order to fully describe the linkage:

$$\mu = \frac{m_2}{m}, \quad \delta = \frac{l_2}{l}, \quad \kappa = \frac{K_{2p}}{K_p}, \quad \sigma = \frac{K_{2d}}{K_d}. \tag{13}$$

The form of equations (2) and (3) remains unchanged, but $\mathbf{H}$, $\mathbf{C}$, $\mathbf{g}$, $\mathbf{u}$, and $\mathbf{D}$ are now expressed in terms of a reduced set of dimensionless parameters, in addition to the system states:

$$\mathbf{H} = \begin{bmatrix} 1 + \mu\delta^2 + 2\,\mu\delta\cos\theta_2 + \mu & \mu\delta^2 + \mu\delta\cos\theta_2 \\ \mu\delta^2 + \mu\delta\cos\theta_2 & \mu\delta^2 \end{bmatrix}, \tag{14}$$

$$\mathbf{C} = \begin{bmatrix} -\mu\delta\dot{\theta}_2\sin\theta_2 & -\mu\delta(\dot{\theta} + \dot{\theta}_2)\sin\theta_2 \\ \mu\delta\dot{\theta}\sin\theta_2 & 0 \end{bmatrix}, \tag{15}$$

$$\mathbf{g} = -\begin{bmatrix} \gamma\{\sin\theta + \mu\delta\sin(\theta + \theta_2) + \mu\sin\theta\} \\ \dfrac{\gamma\,\mu\delta}{\kappa}\{\sin(\theta + \theta_2)\} \end{bmatrix}. \tag{16}$$

The control effort is described by $\mathbf{K}_d = \mathrm{diag}\{2\beta, 2\beta\sigma\}$ and $\mathbf{K}_p = \mathrm{diag}\{1, \kappa\}$.

The disturbance vector $\mathbf{D}(\boldsymbol{\theta}, \boldsymbol{\tau})$ can be expressed as

$$\mathbf{D} = f(\tau)\begin{bmatrix} (1 + \mu)\cos\theta + \mu\delta\cos(\theta + \theta_2) \\ \mu\delta\cos(\theta + \theta_2) \end{bmatrix}, \tag{17}$$

where $f(\tau)$ is as previously defined. For a secondary link of vanishing mass, this case degenerates to the previous, as expected.

As the gravitational torque experienced by the primary link is now substantially influenced by the mass and length of the secondary link, the pre-conditions for global asymptotic stability in the undisturbed case are not necessarily satisfied by all cases of $\gamma < 1$. Examination of the vector **g** reveals that the maximum gravitational torque applied to the primary link is now expressed by $\gamma(1 + \mu\delta + \mu)$, thus producing a shrinking bound on γ as μ and δ increase. As a result, the inequality

$$\gamma(1 + \mu\delta + \mu) < 1 \tag{18}$$

replaces $\gamma < 1$ as a condition for asymptotically stable control in the autonomous, i.e., undisturbed, two-degrees-of-freedom model. Additionally, the control gain of the secondary link has a minimum requirement to offset the payload weight. This can be expressed as $\gamma\mu\delta < \kappa^2$. For convenience, in the later discussion, the derived parameters $\bar{\gamma} = \gamma(1 + \mu\delta + \mu)$ and $\hat{\gamma} = \gamma\mu\delta/\kappa^2$ are introduced here, noting that $\bar{\gamma} < 1$ and $\hat{\gamma} < 1$ now appear as necessary pre-conditions. This added notation is employed only as a clarifying device to better illustrate the relative controller "strength" in the multiple-degrees-of-freedom case. The selection of control parameters in subsequent examples is generally guided by a desire for a near critically damped response for each link in the autonomous case. This performance requirement will typically maintain $\hat{\gamma}$ small. As a result, $\bar{\gamma}$ approaching until will largely be of greater interest.

3. PITCHFORK-TYPE BIFURCATION AND STEADY STATE OFFSET

Governing equation (7) is both non-autonomous and highly non-linear. As a result, an exact, closed-form solution for $\theta(\tau)$ is challenging to obtain, despite the fact that the model possesses only one degree of freedom. Typically, a locally valid solution facilitated by the assumption of small deflection or an approximate solution in terms of a perturbation series [16, 17] is sought as an initial step. Both approaches can be employed to provide a frequency–amplitude response that relates the frequency of the excitation to the amplitude of the steady state oscillation it engenders. A plot of such a relationship predicts substantially diminished steady state oscillation, and thus steady state error, for excitation frequencies much larger than the natural frequency of the system [18]. Such methods, however, are of dubious value here as they completely fail to detect the non-resonant bifurcation of interest and the growth of steady state offset errors.

In this paper, a pitchfork-type bifurcation producing an offset error is documented. While the steady state oscillation will, in large part, conform to the frequency–amplitude prediction by exhibiting diminished amplitude at high excitation frequencies, the position about which this oscillation occurs will be offset from the target state at the origin. Additionally, the magnitude of the offset will tend to *increase* with excitation frequency, typically dwarfing the oscillatory magnitude for the post-bifurcation regime of motion and effectively reversing the trend in overall position error that would otherwise be predicted by the local analysis.

The parameter γ in equation (7) represents the ratio of the maximum gravitationally induced torque to the proportional error signal gain, and, in some sense, is a measure of the relative "strength" of the controller. In the absence of disturbance, the origin remains globally asymptotically stable for all non-negative $\gamma < 1$. In an introductory example, the effect of the time-periodic disturbance $X(t)$ on the usable range of γ is illustrated.

To do so, the system dynamics are examined in the extended phase space. Treating the time scale as a new state variable, the model of equation (7) can be expressed as a third order

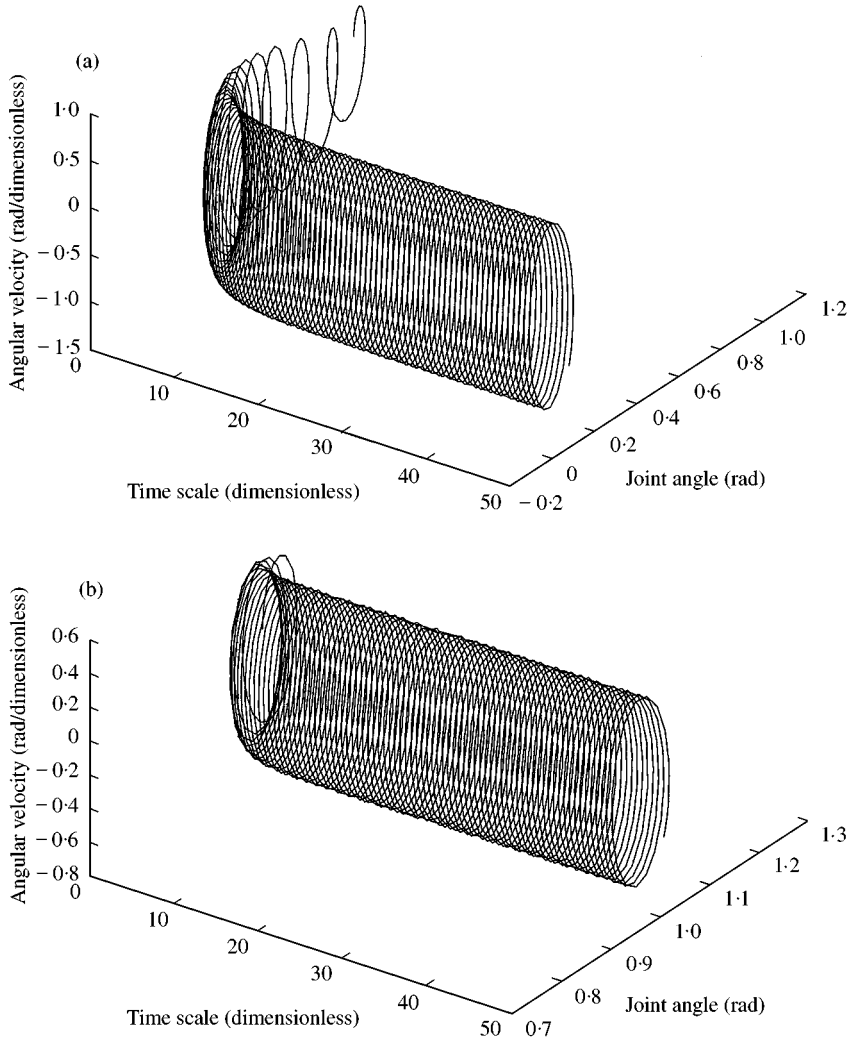

Figure 2. Behavior of controller–plant system in phase space with $\beta = 1{\cdot}00$ when subject to a horizontal base motion of $\alpha = 0{\cdot}100$ and $\Omega = 10{\cdot}0$: (a) $\gamma = 0{\cdot}100$ and (b) 0·900.

autonomous system:

$$\frac{\mathrm{d}}{\mathrm{d}t}\begin{bmatrix}\theta\\ \dot{\theta}\\ \tau\end{bmatrix} = \begin{bmatrix}\dot{\theta}\\ -2\beta\dot{\theta} - \theta + \alpha\Omega^2\cos(\Omega\tau)\cos\theta + \gamma\sin\theta\\ 1\end{bmatrix}. \tag{19}$$

Evolving trajectories can thus be generated in a phase space that possesses a dimension for each state variable.

In Figure 2, the behavior of the controller–plant system is shown for $\gamma = 0{\cdot}100$ and $\beta = 1{\cdot}00$, with a disturbance described by $\alpha = 0{\cdot}100$, and $\Omega = 10{\cdot}0$, for a resting initial condition of 60°. The base vibration causes a steady state oscillation about the target

position at the origin, but the degradation in control performance is not necessarily critical. In the two-dimensional projection of this trajectory onto the phase plane, a limit cycle encircling θ_d results, whose width is on the order of the original disturbance amplitude. As γ is increased to 0·900, however, it can be observed that the long-term motion is no longer centered at the origin, and a large steady state error results. Clearly, the orbit structure of the system is at least partially dependent upon the parameter γ. It will be demonstrated below that the amplitude and frequency of the excitation, α and Ω, respectively, have similar influence. While β has a dramatic impact upon certain qualitative aspects of the control effort, variation in this parameter over a useful range does not appear to produce a similar bifurcation.

In the presence of a time-periodic excitation of the form considered, the steady state motion of the controller–plant system will generally be oscillatory to some degree. Instead of the desired stable equilibrium point, one or more periodic attractors, i.e., limit cycles, will result. If no bifurcation occurs, the amplitude of the steady state oscillation about the origin produces a position error roughly on the order of the original parametric disturbance for non-resonant cases of $\Omega \gg \Omega_N$. As discussed, this error tends to decrease with increasing Ω. When a bifurcation occurs, however, the resulting periodic attractors are offset from the origin, creating a position error that can be of an order of magnitude, or more, greater than the amplitude of the base support vibration.

In Figure 3, bifurcation diagrams are sketched, where the stable steady states are tracked with respect to variations, in turn, of γ, α, and Ω. In each case, β is held at one. When not employed as bifurcation parameters, γ is constant at 0·0750 and Ω is fixed at 10·0. The forcing amplitude α is 0·100 in Figure 3(a) and 0·0500 in Figure 3(b). For reasons of clarity, the branches shown plot the motion of a point on the interior of each stable limit cycle. It should be understood, however, that the motion in the steady state is periodic, and in actually will cover, for a given parameter set, a range of θ in a small neighborhood ε of the plotted point. Explicitly plotting the envelope of oscillation needlessly complicates the otherwise straightforward nature of the bifurcation, however. In general, ε decreases with increasing Ω.

If the varying parameter is generically denoted as λ, it can be seen that for λ less than some critical value, λ_c, a globally stable limit cycle remains at the origin, in the manner discussed. For $\lambda > \lambda_c$, the cycle at the origin is destroyed and two new, symmetrically located, attractors emerge. These branches are labelled S^+ and S^-, respectively, with a discussion of their respective basins of attraction in section 4. The offset error of each grows with increasing λ. It can readily be seen that this is a bifurcation of the pitchfork type, so called for obvious reasons. The bifurcation point, P, occurs at $\lambda = \lambda_c$, though it is important to note that P also exists in a multi-dimensional parameter space.

The consequences of this bifurcation are significant. The rapid increase in the position error for λ in the range immediately following λ_c can quickly degrade controller performance to unacceptable levels. In many cases, the steady state error may well exceed the initial error signal. As a result, the appearance of this pitchfork bifurcation will generally herald control failure.

A more complete picture can be obtained by plotting the location of point P in the parameter space. This is done in Figure 4, where several curves of fixed γ are plotted on the (Ω, α) plane. From the diagram, it can be observed that the orbit structure of the controller–plant system is more sensitive to changes in the excitation frequency at comparatively larger excitation amplitudes. Likewise, threshold values of α and Ω are lowered as γ approaches unity.

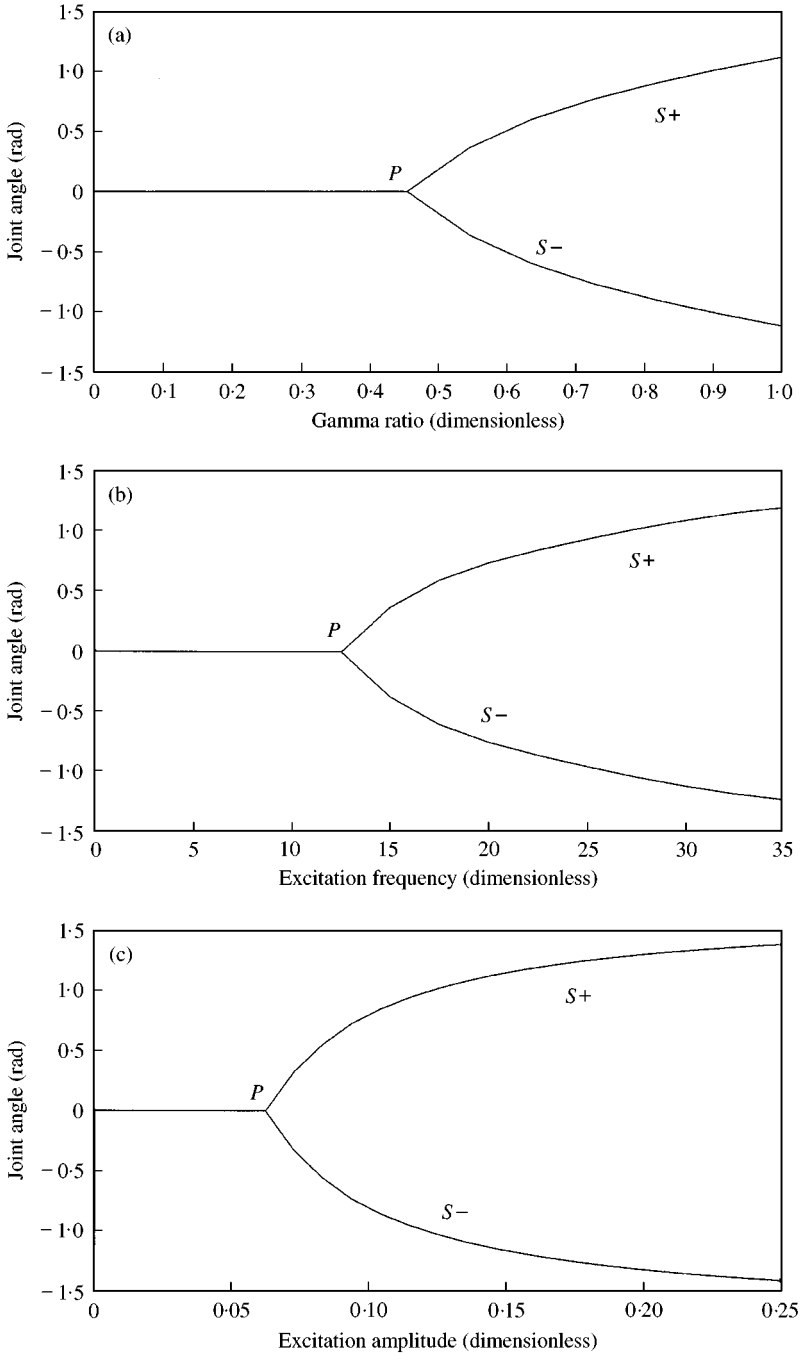

Figure 3. Bifurcation diagrams tracking stable attractors with respect to: (a) γ, with fixed $\alpha = 0{\cdot}100$ and $\Omega = 10{\cdot}0$; (b) Ω, with fixed $\alpha = 0{\cdot}0500$ and $\gamma = 0{\cdot}750$; and (c) α, with fixed $\gamma = 0{\cdot}750$ and $\Omega = 10{\cdot}0$.

In the region above the curve, steady state offset errors of increasing severity will occur. For disturbances of very large amplitude, chaotic oscillations may result. This case is extreme under simple periodic disturbance, however, and will likely be beyond the range of practical consideration for most applications of this model.

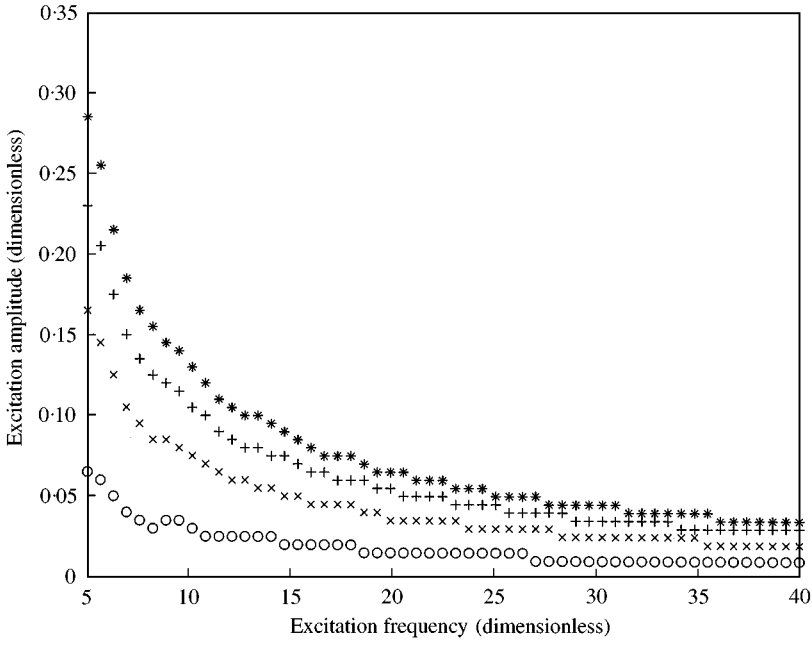

Figure 4. Bifurcation in (Ω, α) plane for various γ, demonstrating increased vulnerability of system with weaker actuation. $*$, $\gamma = 0{\cdot}25$; $+$, $\gamma = 0{\cdot}50$; $\times$, $\gamma = 0{\cdot}75$; o, $\gamma = 0{\cdot}95$.

4. BASINS OF ATTRACTION FOR COMPETING LIMIT CYCLES

In the previous section, the bifurcation and motion of steady state periodic attractors were discussed. However, it is not yet clear which limit cycle will capture orbits evolving from a given initial condition, pre-supposing that the pitchfork bifurcation occurs. The symmetric placement of attractors about the origin can be misleading, as the basins of attraction will not necessarily neatly divide the phase plane.

Consider three trajectories, denoted as φ_a, φ_b, and φ_c, that are at rest at time τ_0 with acute initial positions of a, b, and c, respectively, where $a > b > c > 0$. For a variety of system parameter combinations, a situation can arise where φ_a and φ_c converge to S^+, while φ_b is captured by S^-. Perturbation of parameters from this point can cause φ_b to revert to S^+, or potentially change the steady states of φ_a and φ_c.

The implications are interesting. Firstly, the basins of attraction for the competing periodic attractors are not fixed in shape, and, in fact, may be quite sensitive to variations in system parameters. Secondly, the basins of attraction can become intertwined in certain circumstances. In practical terms, this is a further impediment to achieving the control objective.

Numerical investigation readily reveals that system damping, β, plays a crucial role in the formation of the basins of attraction. In Figure 5, the phase plane of initial conditions is graphically divided between the competing attractors for the case of $\beta = 0{\cdot}250$, $\gamma = 0{\cdot}850$, $\alpha = 0{\cdot}100$, and $\Omega = 10{\cdot}0$. Although the mesh of data points is not exceedingly fine, the effect of decreasing β from 0·250 to 0·0750 is quite clear, as shown in Figure 6. In general, falling β will tend to complicate the partition of the phase plane.

Although the basins of attraction are intertwined in Figure 6, the basin boundary remains smooth and continuous. This is not necessarily the case for under-damped systems with

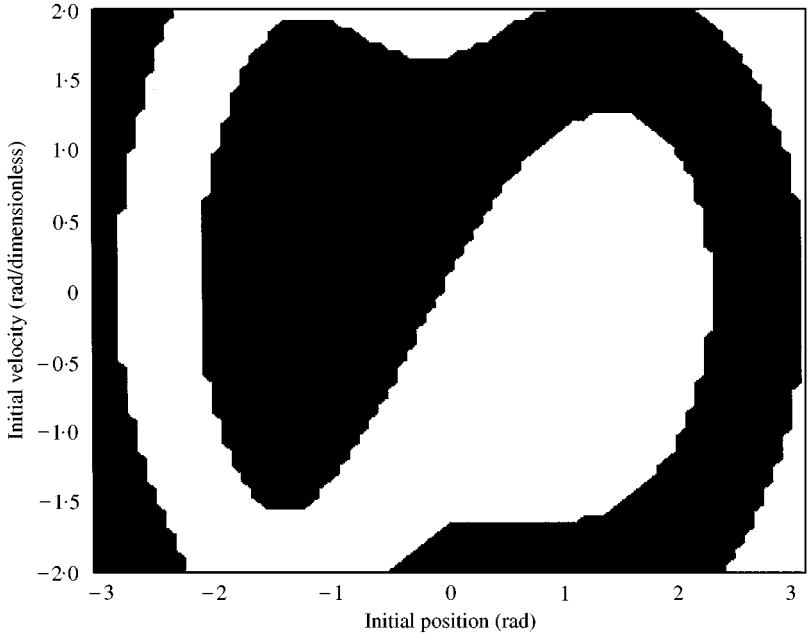

Figure 5. Post-bifurcation basins of attraction for competing limit cycles at $\beta = 0{\cdot}250$ and $\gamma = 0{\cdot}850$.

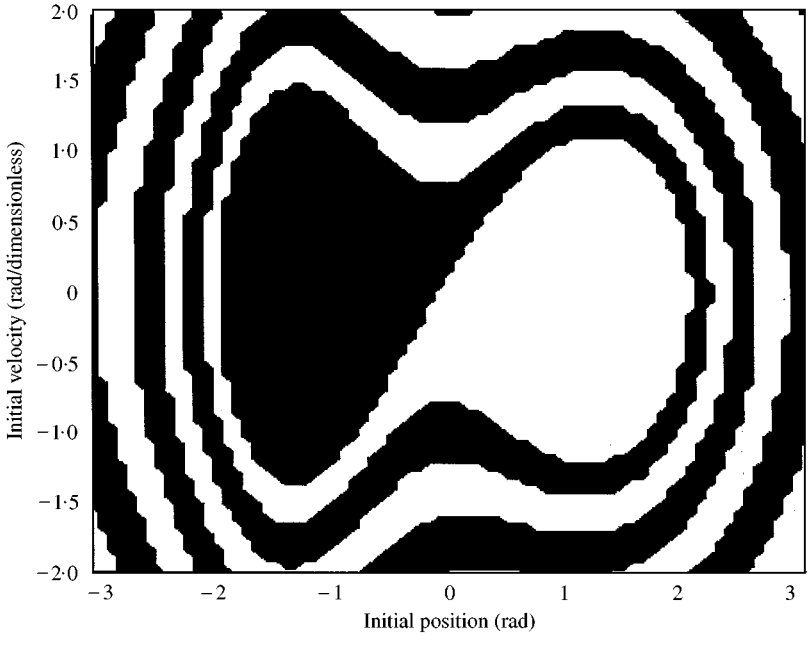

Figure 6. Basins of attraction become more tightly intertwined as β decreased to 0·0750.

sufficient excitation, as shown in Figure 7 for $\beta = 0{\cdot}100$, $\gamma = 0{\cdot}850$, $\alpha = 0{\cdot}200$, and $\Omega = 20{\cdot}0$. Isolated "islands" begin to appear along the boundary, highlighting a localized sensitivity to initial conditions. It is quite possible that fractal basin boundaries [19] may occur in some cases as β continues to decrease. Given relationship (11), β may approach zero much more

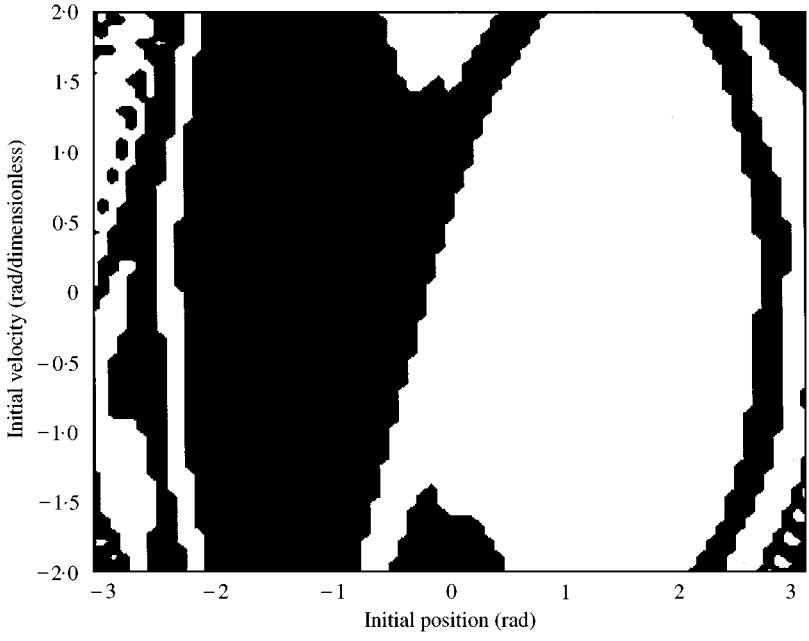

Figure 7. Discontinuous basin boundaries can occur for sufficiently strong disturbances at low damping.

rapidly than ζ for γ near unity. From a control perspective, this issue is largely academic, however, as the motion of the controller–plant system in this regime is already unacceptable with respect to achieving control objectives.

5. BIFURCATION IN MANIPULATOR WITH TWO DEGREES OF FREEDOM

The behavior of the system is now examined for the two-degrees-of-freedom case. At small μ and δ, a close correlation of results between the lower- and higher-dimensional models is observed. The effect of larger payload inertia on the bifurcation point is illustrated by considering links of equal length and mass, i.e., $\mu = \delta = 1{\cdot}00$. The parameters β, κ, and σ are identically set to 1·00, with $\bar{\gamma} = 0{\cdot}750$. The joint-angle error is plotted for each link as a function of the dimensionless time scale for initial conditions at rest. A horizontal base vibration of $\alpha = 0{\cdot}0250$ and $\Omega = 10{\cdot}0$ falls below threshold levels necessary for the pitchfork bifurcation to occur, as shown in Figure 8(a), though the expected low-amplitude steady state oscillation is present. This point can be located on the single-degree-of-freedom bifurcation diagram of Figure 3(c). Increasing α to 0·0500, as in Figure 8(b), produces a noticeable offset, however, that is indicative of a super-critical parameter set with respect to the bifurcation. This point (Ω, α) can be cross-referenced in Figures 3 and 4, where it is *sub-critical* to the bifurcation in each. It is logical to surmise, therefore, that the effect of increasing payload inertia is to lower bifurcation thresholds with respect to disturbance amplitude and frequency.

In Figure 9, a grid of 10 000 points is taken to map the bifurcation boundary in the (Ω, α) parameter plane using output equation (12) and a criterion of steady state payload error greater than 0·500. The control parameters β, κ, and σ are fixed at unity, with $\gamma = 0{\cdot}200$ and $\mu = \delta = 0{\cdot}500$. The shape of the boundary is quite similar to that of Figure 4 in the

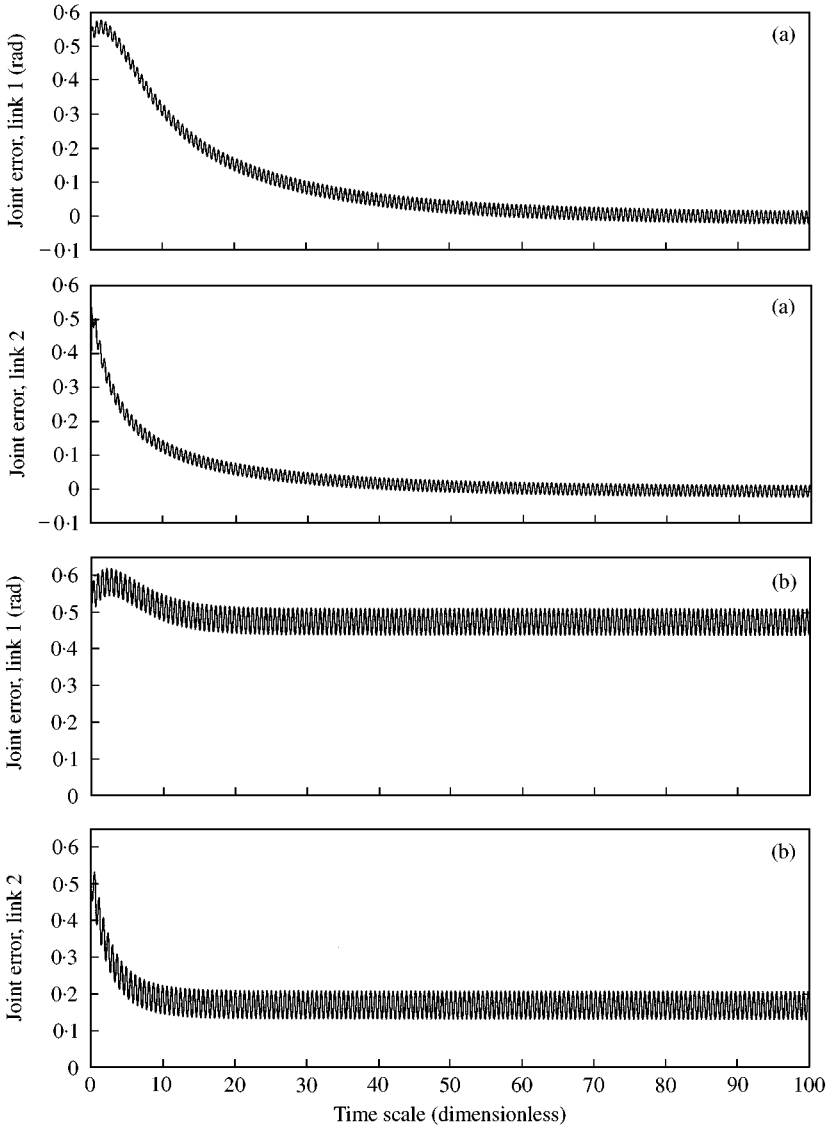

Figure 8. Response of two d.o.f. system with $\mu = \delta = 1{\cdot}00$, $\beta = \kappa = \sigma = 1{\cdot}00$, and $\bar{\gamma} = 0{\cdot}750$ to base vibration indicates that non-vanishing payload inertia lowers bifurcation threshold. In (a) a disturbance with $\alpha = 0{\cdot}0250$ and $\Omega = 10{\cdot}0$ results in an attracting limit cycle encircling the origin, while in (b) an increase to $\alpha = 0{\cdot}0500$ results in steady state offset.

single-degree-of-freedom case, and it can be expected that fluctuations in γ, or $\bar{\gamma}$, will have a similar effect of shifting the boundary up or down slightly. Figure 10 shows the same plot for μ and δ raised to 1·00 at fixed γ, demonstrating the trend for increasing payload inertia. In constructing these two plots we speak of γ fixed, rather than $\bar{\gamma}$, as the latter is dependent upon μ and δ, while the objective is to isolate the influence of payload inertia.

The pitchfork-type bifurcation can occur in the two-degree-of-freedom model for very small disturbance amplitudes, provided the frequency of the excitation is sufficiently large. A benchmark case is shown in Figure 11 for $\alpha = 0{\cdot}0100$ and $\Omega = 50{\cdot}0$. There is a low-amplitude, steady state oscillation about the target state, but no offset error. The

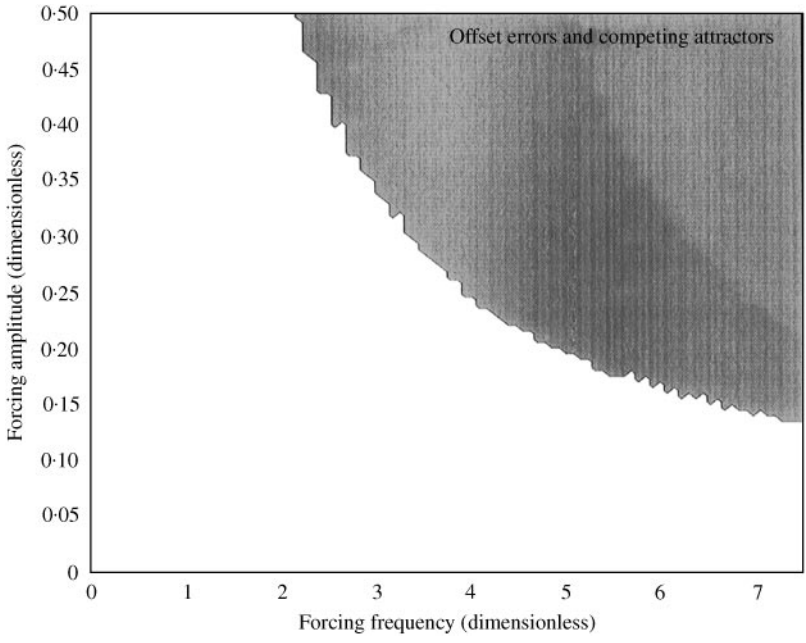

Figure 9. Bifurcation in (Ω, α) parameter plane for two-d.o.f. model with $\mu = \delta = 0{\cdot}500$ and $\beta = \kappa = \sigma = 1{\cdot}00$, based upon total payload error.

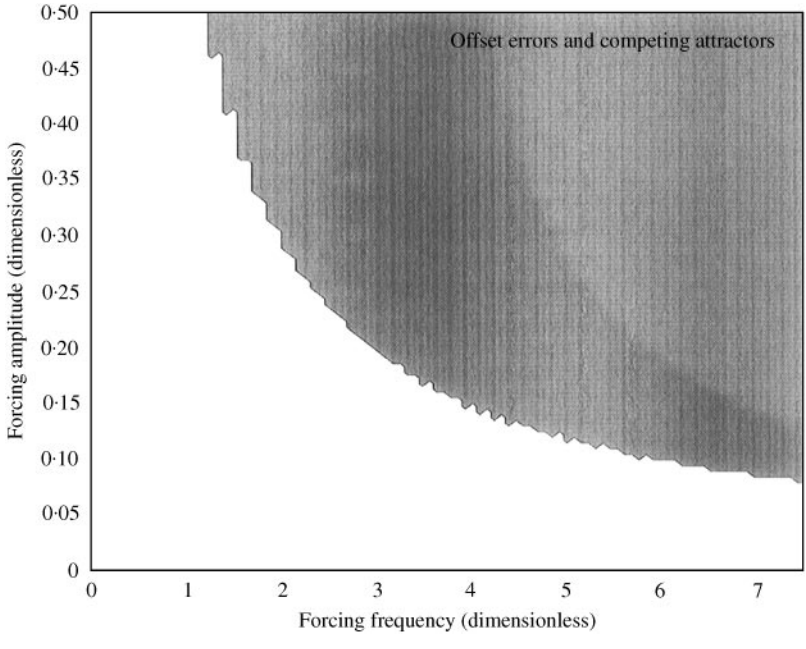

Figure 10. Parameter region dominated by bifurcation increases for $\mu = \delta = 1{\cdot}00$.

comparatively high frequency of the output motion causes the plotted trajectory to appear as a thick line. The bifurcations that result from an increase in Ω to 75·0 at constant α or from an increase in α to 0·0250 at $\Omega = 50{\cdot}0$ are graphed in Figure 12.

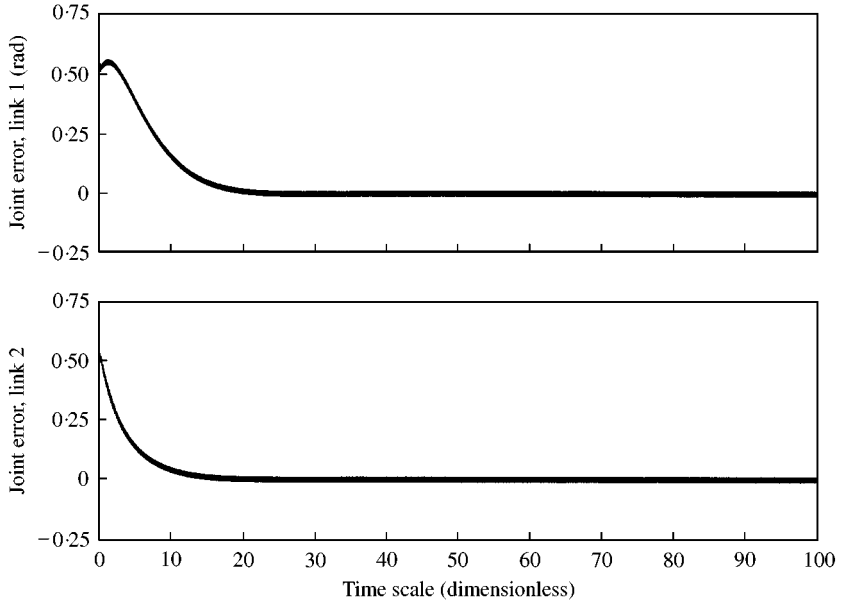

Figure 11. Benchmark response to low amplitude, high-frequency excitation with $\alpha = 0{\cdot}0100$ and $\Omega = 50{\cdot}0$.

The joint-angle offset error observed for the primary link is significantly larger than that for the secondary link. This is not surprising given the form of equation (17), where the secondary link experiences a less severe disturbance. In two degrees of freedom, however, the final position of the payload, or end-effector, is directly dependent upon the joint angle of both links, as described by output equation (12). In practical terms, the Cartesian error of the payload at steady state can be cumulative with respect to the individual joint-angle errors. For higher ordered models, one would expect to see a decrease in the local error of each subsequent link in the aftermath of the discussed bifurcation, but the total error experienced by the payload is likely to remain quite severe.

6. CONCLUSIONS

The analysis presented in this paper demonstrates that a time-periodic parametric excitation, such as that generated by a horizontally vibrating support base, has the potential to seriously impair or degrade the effectiveness of a joint-space, PD-type controller as applied to a robotic manipulator plant, or a generic inverted pendulum. Even for small disturbance amplitudes, a pitchfork-type bifurcation can occur if the excitation frequency is high, or if the ratio of the maximum gravitational torque to the proportional gain is sufficiently close to unity. The offset error introduced by this bifurcation can readily become large and lead to an effective control failure.

The results obtained are significant in comparison to the more commonly examined case of a near-resonant driving excitation. In the latter, low disturbance frequencies near the natural frequency of the system are a concern as the amplitude of steady state oscillation may be amplified. With the disturbance model discussed in this article, however, high-frequency excitation is clearly troublesome, as the steady state *offset error* induced by the bifurcation can easily exceed the amplitude of steady state oscillation by a substantial margin.

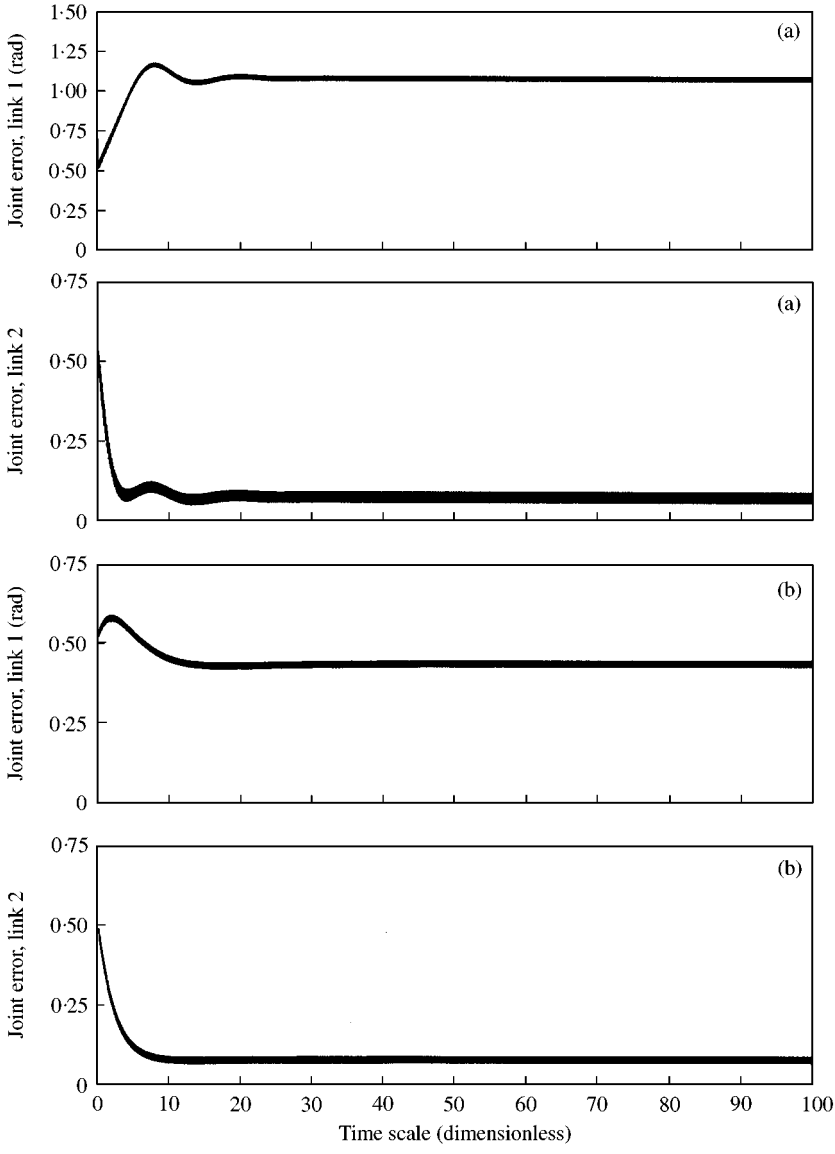

Figure 12. Bifurcation at low disturbance amplitude for (a) $\Omega = 75{\cdot}0$ at $\alpha = 0{\cdot}0100$ and (b) $\alpha = 0{\cdot}0250$ at $\Omega = 50{\cdot}0$.

The appearance of symmetric, offset, periodic attractors is not restricted to cases of impractically low damping. The simulations included demonstrate that the bifurcation can occur in over-damped systems as well. In fact, the location of the bifurcation point does not appear to be sensitive to system damping via the parameter β. This ratio does, however, have a significant impact on the basins of attraction for the competing limit cycles that occur following the bifurcation. Low β can produce intertwined basins of attraction, while a highly under-damped system can yield localized sensitivity to initial conditions.

Given a typical output relation where the Cartesian co-ordinates of the payload, and not just its angular orientation, are important, it can readily be observed that a two-degrees-of-freedom model is susceptible to the same sort of bifurcation. Although the angular offset

experienced by the secondary link is smaller than that of the primary link, the total error in the position of the payload is derived from a combination of the two within the joint-space framework. On this basis, and that of the simulations presented, it is reasonable to suspect that higher ordered linkages may also evidence sensitivity to parametric excitations of the sort discussed.

REFERENCES

1. E. GWINN and R. WESTERVELT 1985 *Physical Review Letters* **54**, 1613–1616. Intermittent chaos and low-frequency noise in the driven damped pendulum.
2. M. S. SOLIMAN 1996 *International Journal of Non-Linear Mechanics* **31**, 167–174. Jump phenomena resulting in unpredictable dynamics in the driven, damped pendulum.
3. R. W. LEVEN and B. P. KOCH 1981 *Physics Letters A* **86**, 71–74. Chaotic behavior of a parametrically excited damped pendulum.
4. J. MCLAUGHLIN 1981 *Journal of Statistical Physics* **24**, 375–388. Period doubling bifurcations and chaotic motion for a parametrically forced pendulum.
5. A. S. RAVISHANKAR and A. GHOSAL 1999 *International Journal of Robotics Research* **18**, 93–108. Nonlinear dynamics and chaotic motions in feedback controlled two and three degree-of-freedom robots.
6. S. LANKALAPALLI and A. GHOSAL 1996 *Proceedings of the* 1996 *IEEE International Conference on Robotics and Automation, Minneapolis*, Vol. 2, 1241–1245. Possible chaotic motions in a feedback controlled 2R robot.
7. V. MAHOUT, P. LOPEZ, J. CARCASES and C. MIRA 1993 *IEEE International Conference On Systems, Man, and Cybernetics, Le Touquet, France*, 201–205. Complex behaviors of a two revolute joints robot: harmonic, subharmonic, higher harmonic, fractional harmonic, chaotic responses.
8. R. SEYDEL 1994 *Practical Bifurcation and Stability Analysis: From Equilibrium to Chaos*, 45–107. New York: Springer-Verlag.
9. M. W. SPONG and M. VIDYASAGAR 1989 *Robot Dynamics and Control*. New York: John Wiley and Sons.
10. M. TAKEGAKI and S. ARIMOTO 1981 *American Society of Mechanical Engineers Journal of Dynamic Systems, Measurement, and Control* **103**, 119–125. A new feedback method for dynamic control of manipulators.
11. R. KELLY 1997 *International Journal of Robotics Research* **16**, 660–672, PD control with desired gravity compensation of robotic manipulators: a review.
12. S. ARIMOTO 1996 *Control Theory of Nonlinear Systems: A Passivity Based and Circuit-Theoretical Approach*. Oxford: Oxford University Press.
13. W. FENG and I. POSTLETHWAITE 1993 *International Journal of Robotics Research* **12**, 490–496. A simple robust control scheme for robot manipulators with only joint position measurements.
14. L. BLITZER 1965 *American Journal of Physics* **33**, 1076–1078. Inverted pendulum.
15. H. NIJMEIJER and A. VAN DER SCHAFT 1990 *Non-Linear Dynamical Control Systems*, 349–355. New York: Springer-Verlag.
16. J. SANDERS and F. VERHULST 1985 *Averaging Methods in Non-Linear Dynamical Systems*. New York: Springer-Verlag.
17. M. HOLMES 1995 *Introduction to Perturbation Methods*, 105–153. New York: Springer-Verlag.
18. S. TIMOSHENKO, D. YOUNG and W. WEAVER 1974 *Vibration Problems in Engineering*, 176–186. New York: John Wiley and Sons: fourth edition.
19. F. MOON 1987 *Chaotic Vibrations: An Introduction for Applied Scientists and Engineers*, 242–257. New York: John Wiley and Sons.